






Article

Innovative Photocatalytic Reactor for Sustainable Industrial Water Decontamination: Utilizing 3D-Printed Components and Silica-Titania Trilayer Coatings

George V. Theodorakopoulos ^{1,2,*} , Michalis K. Arfanis ^{1,2} , Tadej Stepišnik Perdih ², Simos Malamis ² , Dimitrios Iatrou ³, George Em. Romanos ¹  and Polycarpos Falaras ^{1,*} 

¹ Institute of Nanoscience and Nanotechnology, National Center for Scientific Research “Demokritos”, Agia Paraskevi, 15341 Athens, Greece; m.arfanis@inn.demokritos.gr (M.K.A.); g.romanos@inn.demokritos.gr (G.E.R.)

² Sanitary Engineering Laboratory, Department of Water Resources and Environmental Engineering, School of Civil Engineering, National Technical University of Athens, Zografou, 15780 Athens, Greece; tadej.stepisnik@gmail.com (T.S.P.); malamis.simos@gmail.com (S.M.)

³ IAMAS Technologies Ltd., 128 City Road, London EC1V 2NX, UK; iatrou.iamas@gmail.com

* Correspondence: g.theodorakopoulos@inn.demokritos.gr (G.V.T.); p.falaras@inn.demokritos.gr (P.F.); Tel.: +30-210-650-3977 (G.V.T.); +30-210-650-3644 (P.F.)

Abstract: Industrial activities generate enormous quantities of polluted effluents, necessitating advanced methods of wastewater treatment to prevent potential environmental threats. Thus, the design of a novel photocatalytic reactor for industrial water decontamination, purification, and reuse is proposed as an efficient advanced oxidation technology. In this work, the development of the active reactor components is described, utilizing a two-step sol-gel technique to prepare a silica-titania trilayer coating on 3D-printed polymeric filters. The initial dip-coated SiO₂ insulator further protects and enhances the stability of the polymer matrix, and the subsequent TiO₂ layers endow the composite architecture with photocatalytic functionality. The structural and morphological characteristics of the modified photocatalytic filters are extensively investigated, and their performance is assessed by studying the photocatalytic degradation of the Triton X-100, a common and standard chemical surfactant, presented in the contaminated wastewater of the steel metal industry. The promising outcomes of the innovative versatile reactor pave the way for developing scalable, cost-effective reactors for efficient water treatment technologies.

Keywords: 3D printing; filters; titania; photocatalysis; Triton X-100; wastewater treatment



Citation: Theodorakopoulos, G.V.; Arfanis, M.K.; Stepišnik Perdih, T.; Malamis, S.; Iatrou, D.; Romanos, G.E.; Falaras, P. Innovative Photocatalytic Reactor for Sustainable Industrial Water Decontamination: Utilizing 3D-Printed Components and Silica-Titania Trilayer Coatings. *Environments* **2024**, *11*, 156. <https://doi.org/10.3390/environments11070156>

Academic Editors: Zhen Wei, Yueping Bao and Wenlu Li

Received: 28 May 2024
Revised: 15 July 2024
Accepted: 18 July 2024
Published: 20 July 2024



Copyright: © 2024 by the authors. Licensee MDPI, Basel, Switzerland. This article is an open access article distributed under the terms and conditions of the Creative Commons Attribution (CC BY) license (<https://creativecommons.org/licenses/by/4.0/>).

1. Introduction

The deterioration of water quality due to environmental pollution has become a significant concern [1,2], causing an urgent need for effective treatment [3–6], purification [7,8], and reclamation [9–12] of water and industrial wastewater. This has prompted the exploration of various innovative and sustainable methods for water treatment. Thus, to address these challenges and minimize pollution in both municipal and industrial effluents, strict regulations and technological advancements are being promoted. Stringent regulations and policies must be implemented to control the discharge of pollutants into water bodies, thereby alleviating the burden on water treatment systems. On the other hand, among the proposed solutions, Advanced Oxidation Technologies (AOTs) and Advanced Reduction Technologies (ARTs), as highlighted in the literature [13], offer promising avenues for combating water pollution. These technologies can be seamlessly integrated into existing infrastructures without the need for overly complex processes or the addition of harmful chemical reagents. Herein, photocatalysis, a process of utilizing light to accelerate a reaction, has emerged as a promising solution for various environmental, industrial, and energy applications. Titanium dioxide (TiO₂), also referred to as titania, is distinguished among

photocatalysts due to its exceptional properties such as stability, non-toxicity, abundance, and cost-effectiveness [14–16]. The photocatalytic activity of TiO₂ arises from its ability to generate electron–hole pairs when exposed to light irradiation, enabling them to participate in redox reactions with species adsorbed on its surface [14,16,17].

To date, laboratory-scale and pilot-scale reactors utilizing the photocatalytic properties of titania catalysts have exhibited considerable potential for future applications in wastewater management, as evidenced in the literature [18–20]. Specifically, recent research has extensively explored the application of TiO₂ in both laboratory-scale and larger pilot-scale reactors [19,21–28]. Laboratory-scale reactors provide a controlled environment aiding in understanding the fundamental mechanisms of photocatalysis and optimizing parameters and catalyst properties. This also enables the exploration of innovative reactor designs with precise control over experimental parameters. Conversely, pilot-scale reactors serve to validate the scalability and feasibility of photocatalytic processes under more realistic conditions, including complex feed compositions, varying light intensities, and higher treated volumes. Developing effective pilot-scale reactors entails addressing challenges such as photon penetration depth due to the increase in light path length through the reactor [29], reactor geometry [30], limitations in mass transfer between reactants to the photocatalyst surface [25,31,32], stability of photocatalysts [33], economic feasibility [34], and strategies for immobilizing catalysts [35,36]. Despite these challenges, the potential benefits of photocatalysis in addressing environmental and energy-related issues render it a promising technology for diverse environmental applications.

In line with these advancements, a novel approach involves the development of a 3D-printed photocatalytic filtration reactor (3D-PFR) tailored for wastewater purification and reuse, with a steel metal industry serving as a case study. The core innovation lies in the deposition of titanium dioxide photocatalysts onto 3D-printed flat polymeric filters. These bespoke structured photocatalysts are integrated into a continuous flow photocatalytic reactor, thus advancing a patented hybrid technology for water treatment that combines filtration and photocatalytic degradation processes. This versatile design enables cost-effective reactor manufacturing while facilitating parallel operational performance optimization and scalability.

2. Materials and Methods

2.1. Lattices Fabrication and Preparation of Trilayer Coatings

Initially, the polymeric flat filters in the form of lattices were fabricated utilizing Digital Light Processing (DLP) 3D-printing technology, employing the appropriate resins, software, and hardware equipment. The resulting 3D-printed lattices (Figure 1a) measured 21.4 mm in width, 4 mm in depth, and 21 mm in height, exhibiting a significant aspect ratio with volume and surface area values of 781.9 mm³ and 6801 mm², respectively. Additionally, scale-up rectangular lattices measuring 16.5 cm in width and height were produced, similarly boasting an enhanced aspect ratio. The deposition of the silica-titania trilayer coatings was carried out in three sequential steps using straightforward and facile sol-gel dip-coating techniques.

In this context, the deposition conditions of a silica-titania trilayer coating were precisely optimized and assessed for their efficacy in photocatalytic processes [37]. In brief, initially, a silica (SiO₂) inert protective layer was applied to the membranes prior to the addition of TiO₂. This step aimed to enhance robustness, prevent undesirable polymer degradation effects, and improve the catalyst's adhesion to the tiles (lattices). The photocatalytic activation process involved immersing the membranes in a TiO₂ precursor solution, followed by thermal treatment under ambient conditions [38]. The final TiO₂/P25 layer was formed on the modified lattices by dispersing the commercial Evonik Aeroxide TiO₂ P25 photocatalyst into the aforementioned titania precursor solution and repeating the dipping and annealing steps.

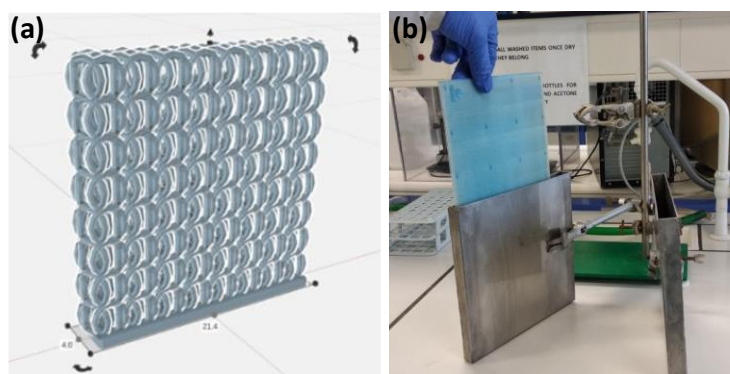


Figure 1. (a) 3D-printed flat filter of high surface area; (b) deposition of the final $\text{TiO}_2/\text{P25}$ coating onto the filter.

More specifically, as aforementioned, initially, the silica layer was applied using the sol-gel dip-coating technique. The lattice was submerged in a SiO_2 precursor solution with precise control over both the dipping and withdrawal speeds employing a dip coater (Ossila Ltd., Sheffield, UK). Subsequently, the treated lattice was dried under mild conditions at room temperature and low humidity for a day. After several trials, the final optimized silica precursor solution comprised ethanol, tetraethyl orthosilicate (TEOS), water, and HCl, with a molar ratio of 1: 37:4:5.5 $\times 10^{-2}$ [37].

The outer titania layer was also applied using the sol-gel dip-coating technique, with careful control over the dipping and withdrawal speeds. Following the preparation of the silica coating, the lattice was immersed in the TiO_2 precursor solution. The initial colloidal solution was prepared by dissolving titanium isopropoxide (TTIP) (15 mL) in ethanol (2.5 mL). Next, the peptizing agent was formulated by slowly adding 1 mL of perchloric acid (HClO_4) to 45 mL of ultrapure water (Milli-Q, 18 $\text{M}\Omega\cdot\text{cm}$), and was then gradually introduced into the mixed-metal alkoxide solution. The exothermic hydrolysis of TTIP produced an amorphous white precipitate. Following refluxing for 48 h at $\sim 70^\circ\text{C}$ to promote crystallization, a stable primary sol was achieved [39]. Once cooled down to room temperature (RT), the flat SiO_2 -coated lattices were immersed in the final solution to form the TiO_2 coating. Subsequently, after dip-coating, the samples were dried using a blow-dryer for approximately 30 s on each side from a distance of approximately 30 cm.

An additional layer with $\text{TiO}_2/\text{P25}$ coating was prepared by dispersing the commercial TiO_2 photocatalyst Evonik Aeroxide P25 (1 g) into the aforementioned titania precursor solution (30 mL). Subsequently, the same dip-coating procedure was carried out (Figure 1b). Additionally, all the coated samples underwent post-annealing at 150°C for 3 h. The final applied layer was implemented to ensure that the TiO_2 top layer would contain a significant proportion of the anatase phase, known for its enhanced photocatalytic activity. This was necessary because the post-annealing at 150°C (the maximum temperature limited by the thermal endurance of the polymeric lattice) was insufficient to convert the amorphous TiO_2 coating into the photoactive, crystalline anatase phase.

Pristine, SiO_2 -, bilayer-, and trilayer-modified polymeric lattices underwent comprehensive characterization using microscopic and spectroscopic techniques to determine the morphological and structural characteristics of the photocatalyst.

2.2. Accelerated Aging Tests

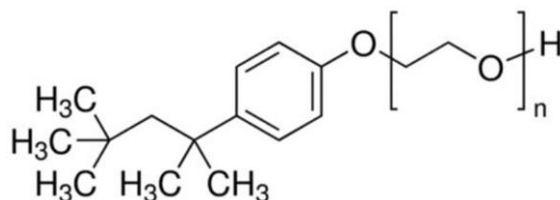
The conduction of the accelerated aging tests encompassed chemical, irradiation, and thermal assessments. Specifically, regarding the chemical aging resistance of the 3D-printed flat membranes, they underwent 24 h immersion in an acidic solution of HNO_3 (pH ~ 5), followed by an equivalent duration in an alkaline solution of KOH (pH ~ 8). The irradiation tests comprised 24 h exposure to UV-A light, while the evaluation of the thermal endurance involved 3 h of soaking time at 150°C .

2.3. Characterization Techniques

The structural characterization of the lattice and coatings was conducted using X-ray diffraction (XRD) analysis, employing a Siemens D-500 diffractometer (Siemens, Erlangen, Germany). This analysis utilized Cu Ka1 ($\lambda = 1.5406 \text{ \AA}$) and Ka2 ($\lambda = 1.5444 \text{ \AA}$) radiation. Additionally, vibrational Raman spectroscopy measurements were performed using a Renishaw inVia Reflex spectrometer (Renishaw, Wotton-under-Edge, UK) equipped with a solid-state laser emitting at 514.5 nm, along with a Leica DMLC microscope with a $\times 50$ lens. The morphology of the lattice and coatings was examined using a FEI Quanta-Inspect scanning electron microscope (SEM) with a tungsten filament operating at 25 kV (FEI Company, Eindhoven, The Netherlands), coupled with an energy-dispersive X-ray spectrometer (EDS). The surface hydrophilicity of the lattices was evaluated using a contact angle meter (CAM 100, KSV Instruments Ltd., Helsinki, Finland). For static contact angle measurements, deionized water (5 μL) was used for the sessile drop type, and the affinity of the drop with the surface was assessed using a software fitting method. Ten measurements were collected from different spots on the lattice at room temperature (20 $^{\circ}\text{C}$), and the mean contact angle and standard deviation were calculated. A TGA/DTA Thermogravimetric/Differential Thermal Analyzer (Setsys Evolution 18, Setaram Instrumentation, Caluire, France) and differential scanning calorimetry (DSC) were utilized to examine the thermal characteristics of the polymer lattice.

2.4. Photocatalytic Performance

Preliminary experiments involved comparing different nanoparticulate TiO_2 powders with commercial Evonic P25 to assess the performance of the synthesized powders. Subsequently, the photocatalytic efficiency of trilayer coatings on lattices was evaluated by studying the photodegradation of the organic non-ionic surfactant Triton X-100 (Scheme 1) at various concentrations.



Scheme 1. The molecular structure of Triton X-100 [Formula: $\text{C}_{14}\text{H}_{22}\text{O}(\text{C}_2\text{H}_4\text{O})_n$ ($n = 9\text{--}10$)].

These lattices were placed into specially designed custom-made cells, and the photocatalytic experiments were conducted in a rectangular parallelepiped black box photoreactor (50 cm \times 40 cm \times 30 cm) under UV-A illumination, as previously described in detail [40]. The cells were positioned 15 cm away from the illumination system. The reactor was equipped with four Sylvania GTE F15W/T8UV-A lamps, emitting light in the 350–390 nm range with an intensity of $0.5 \text{ mW}\cdot\text{cm}^{-2}$, arranged in a parallel symmetric configuration atop the reactor. Photocatalytic kinetics were monitored by measuring the characteristic absorption peak of Triton X-100 at 224 nm using a Hitachi 3010 UV-Vis spectrophotometer), equipped with an integrating sphere and BaSO_4 as the reference (Hitachi Ltd., Tokyo, Japan). Measurements were taken every 30 min over a total duration of 90 min. Before illumination, the solutions were allowed to equilibrate in the dark for 30 min to ensure adsorption–desorption equilibrium of the surfactant onto the photocatalyst. The photodegradation efficiency (%) was subsequently determined by the following equation:

$$\frac{\Delta C}{C_0} (\%) = \left(\frac{C_0 - C}{C_0} \right) \times 100\% \quad (1)$$

where C_0 is the pollutant concentration after the adsorption equilibrium (mg/L) and C represents the concentration at any time during the experiment (mg/L).

Similarly, to determine the extent of mineralization during the photocatalytic degradation process, total organic carbon (TOC) measurements were performed employing a TOC analyzer (BioTector B3500, Hach, Loveland, CO, USA), and the carbon removal efficiency (%) was calculated using the following equation:

$$\frac{\Delta\text{TOC}}{\text{TOC}_0}(\%) = \left(\frac{\text{TOC}_0 - \text{TOC}}{\text{TOC}_0} \right) \times 100\% \quad (2)$$

where TOC_0 is the pollutant's organic carbon concentration after the adsorption equilibrium (mg/L) and TOC denotes the organic carbon concentration at any time during the experiment (mg/L).

3. Results

3.1. Accelerated Aging Results

As described in Section 2.2, the lattices underwent physical testing, being subjected to unusually high levels of chemical (Figure 2a), irradiation (Figure 2b), and thermal stress to accelerate natural aging effects. As depicted in Figure 2c, it was determined that neither chemical stress (at pH 5 and pH 8) nor irradiation (UVA 365 nm) stress significantly altered the morphology and chemistry of the polymeric lattices. However, a slight color change observed under UV irradiation prompted us to decide on depositing a protective SiO_2 layer beneath the photocatalytic TiO_2 layer.

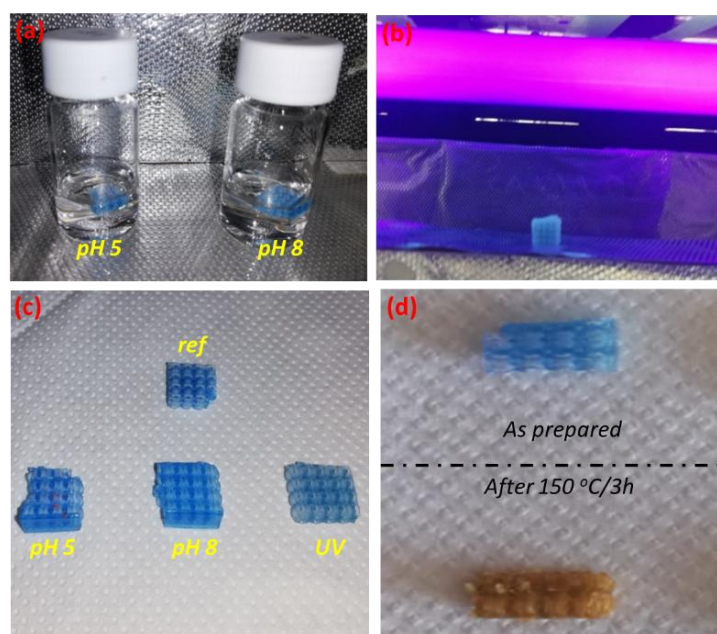


Figure 2. (a) Chemical and (b) irradiation stress testing in progress; (c) appearance of the small-scale lattices after chemical and irradiation stress testing; (d) appearance of the lattice after thermal annealing.

Following thermal stress (annealing for 3 h at 150 °C), the samples' color changed from light blue to light yellow (Figure 2d). The Raman spectrum, as shown in Figure 3a, remained unchanged, indicating that the substrate was fabricated from Bisphenol A diglycidyl ether (DGEBA) epoxy resin, despite the emergence of a luminescent background. Moreover, exothermic events revealed in the TGA curve and DSC thermogram (Figure 3b) of the developed lattices show that the onset of thermal decomposition of the DGEBA epoxy resin might start above 120 °C, potentially impacting the polymer.

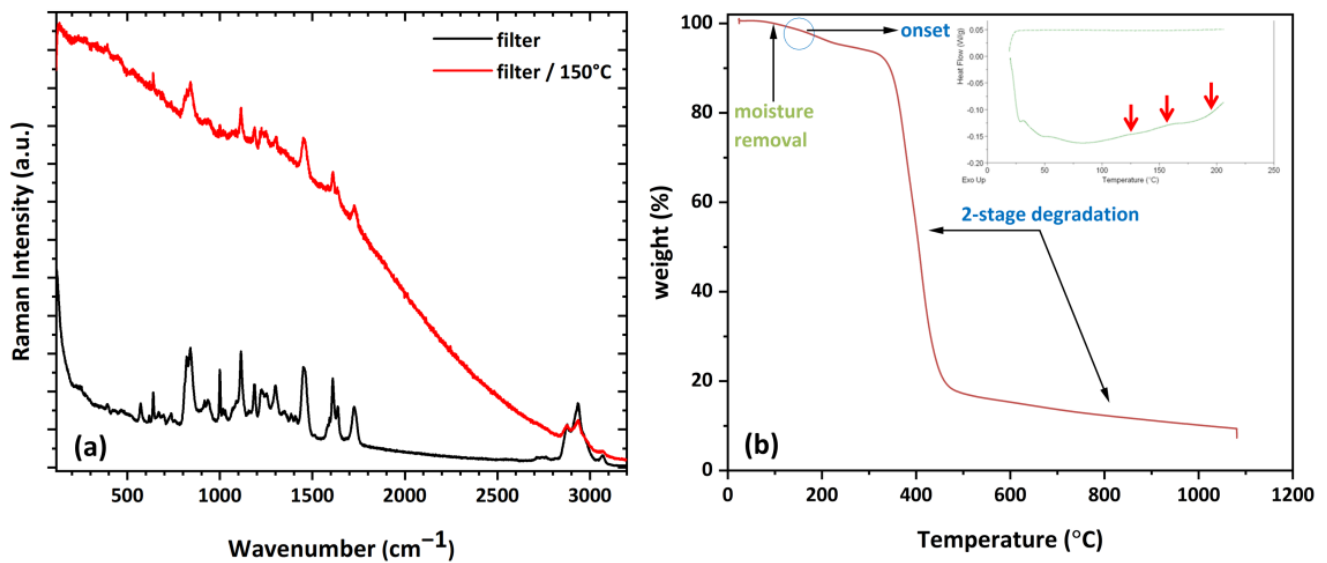


Figure 3. (a) Comparison of the Raman spectra of the developed lattice and that after thermal annealing at 150 °C; (b) TGA curve of polymer lattice; in inset, the DSC thermogram of polymer lattice is depicted.

Furthermore, SEM was employed to observe the morphological features of the lattices both before and after the stress tests. Consequently, minor alterations on the polymer's surface were noticed following immersion in solutions of varying pH. However, it cannot be definitively stated that the material remains unaffected after undergoing the thermal stress test. Specifically, although the initially prepared 3D-printed lattices exhibited a highly uniform and smooth structure (with any random grains possibly arising from the Au sputtering), localized cracks emerged after 3 h of annealing at 150 °C (Figure 4).

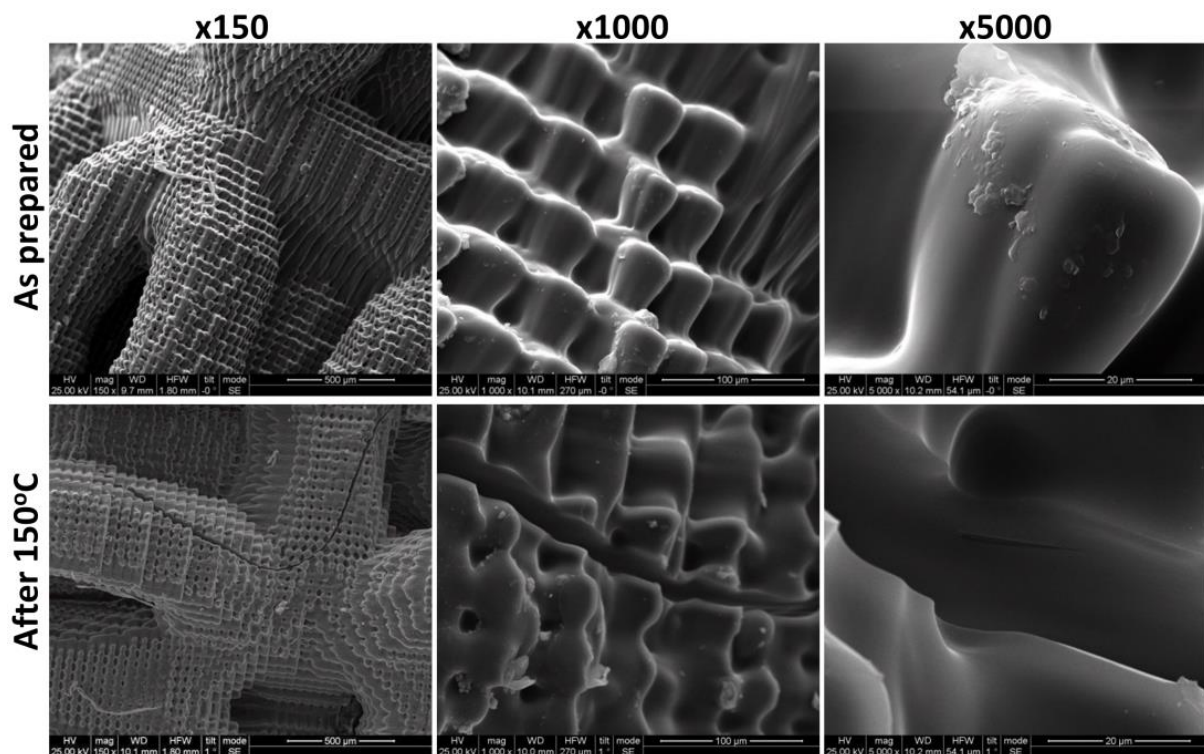


Figure 4. SEM images obtained at various magnifications for the untreated and thermally annealed lattice at 150 °C.

The general remarks from the stress tests conducted on the polymeric lattices, which serve as substrates for the development of the photocatalytic coatings, indicate that there are no discernible alterations following exposure to acidic and alkaline environments or UV irradiation. However, thermal stress indeed affected the membrane morphology. Consequently, thermal post-treatment under mild conditions may be considered subsequent to the deposition of SiO_2 and TiO_2 films.

3.2. Morphological Study of the Trilayer Coated Lattices

As aforementioned in Section 2.1 (Lattices fabrication and preparation of trilayer coatings), adjusting and optimizing the TEOS-to-HCl ratio resulted in a smooth and defect-free coating on the lattice surface with the elimination of any crack formation (Figure 5a). In addition, as indicated in the third column of Figure 5a, the quality of the coating was not affected by the duration of solution curing.

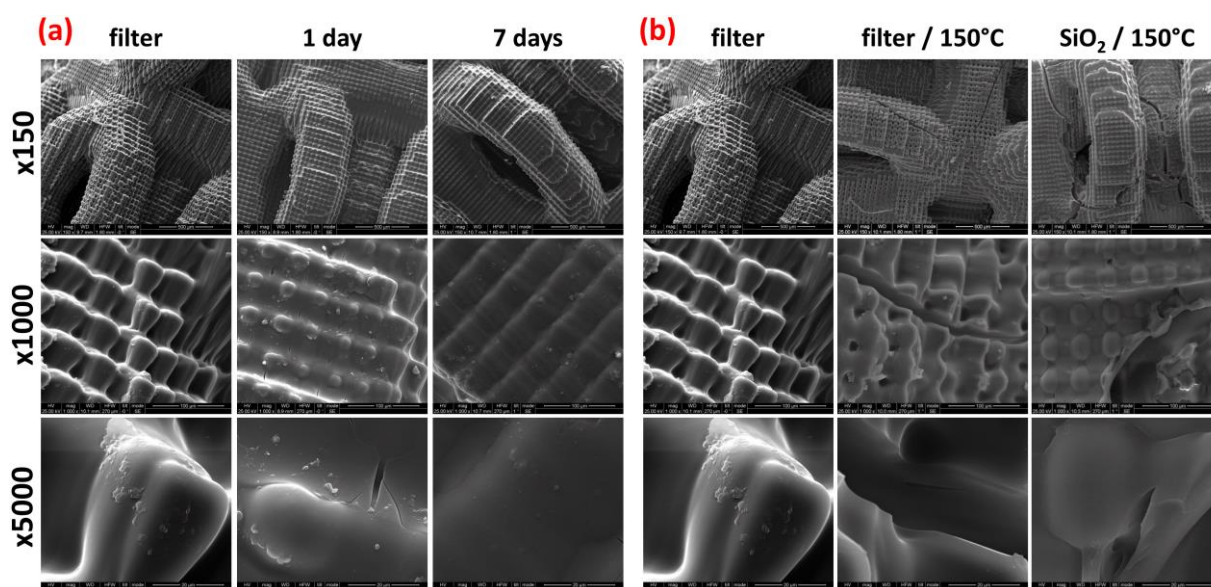


Figure 5. (a) The morphology of the SiO_2 layer on the lattice surface, prepared using the dip-coating technique, after one- and seven-days of solution curing; (b) SEM images of the untreated and heat-treated lattice and the heat-treated SiO_2 -coated lattice.

Additionally, the SEM micrographs in Figure 5b indicated that the morphology of the SiO_2 coating remained unchanged after post-annealing at 150 °C, smoothly covering the surface without inducing additional cracks. It should also be noted that despite the significant cracks in the polymer after annealing (Figure 5b, middle column), the SiO_2 coating remained intact. This suggests that the SiO_2 coating acts as a mending agent for cracks developed in the polymeric lattice under thermal stress at 150 °C.

Subsequently, a comprehensive examination of the layer-by-layer coating morphology using SEM (Figure 6) confirmed the presence of a 3D honeycomb-like structure of the flat filters. Practically, the resolution capabilities of the 3D printer allow for the construction of the desired filter by printing micro-sized “bricks” (with dimensions of $16 \mu\text{m} \times 16 \mu\text{m} \times 34 \mu\text{m}$) as the pattern for building blocks. As mentioned before, the subsequent application of the SiO_2 layer resulted in a very uniform, homogenous, and smooth coverage, maintaining the initial surface roughness to a significant extent. Despite some minor imperfections that appeared on the surface, the high quality of the SiO_2 layer ensures the efficient insulation of the polymeric substrate and improved adhesion of the top TiO_2 coating. In addition, as can be observed, the substrate is completely covered by the thicker titania coating. The cracks in the TiO_2 did not compromise the stability of the polymer, due to the insulation provided by SiO_2 . Upon adding Evonik P25 into the titania precursor solution, the coating morphology remains unchanged, except for the addition

of white large grains incorporated onto the external surface. The P25 powder ultimately resulted in random grains ranging in size from 160 to 700 nm.

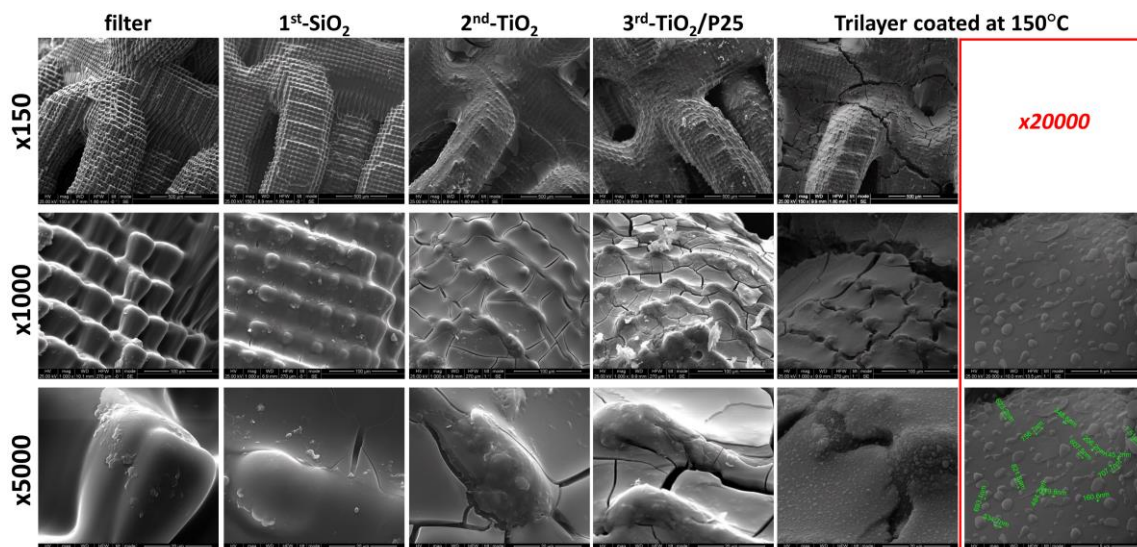


Figure 6. SEM images of 3D-printed flat lattice; together with the top SiO₂, TiO₂, and TiO₂/P25 layers after post-annealing at 150 °C.

The energy-dispersive X-ray spectroscopy (EDS) analysis indicates that upon application of the SiO₂ coating, a pronounced peak from elemental Si was detected, as observed in Figure 7 (left). The addition of TiO₂ leads to overlap with the SiO₂ layer, as Ti coexists with the reduced Si peak (Ti signal low in Figure 7—middle). Following the application of the P25 coating, elemental Ti emerges as the predominant element on the lattice surface, as clearly depicted in Figure 7 (right).

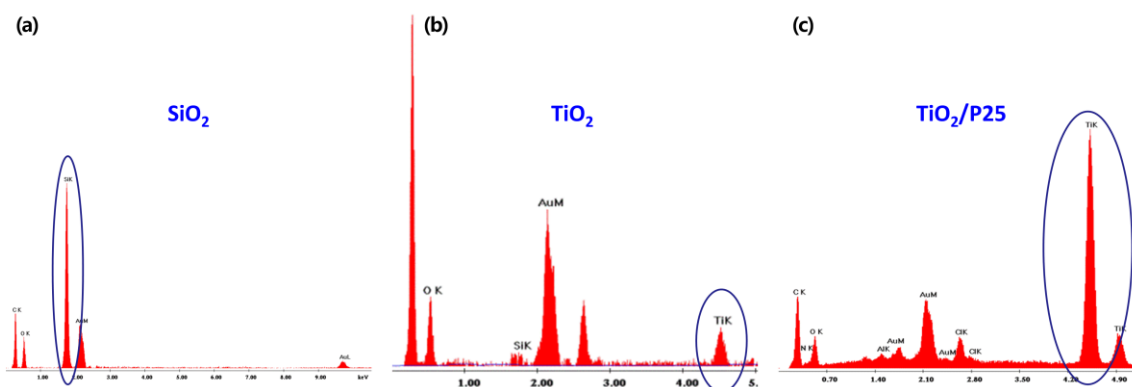


Figure 7. EDS spectra of coated 3D-printed flat lattice with the top (a) SiO₂; (b) TiO₂; and (c) TiO₂/P25 layers.

3.3. XRD Analysis

The XRD analysis of the lattices indicated that the polymeric matrix solely exhibited a broad diffraction peak at approximately 20° (Figure 8), a common characteristic observed in many polymeric materials. The absence of any SiO₂ or TiO₂ peaks suggests their uniform and high dispersion of coatings on the membrane surface. Another remark is that the XRD pattern did not exhibit any Bragg peaks associated with crystalline TiO₂, likely due to the low TiO₂ content, which could not be detected on the polymeric substrate. This outcome is favorable, indicating the formation of an ultra-thin TiO₂ film. An ultra-thin film is advantageous as it maintains the high surface area of the photocatalytic filter and helps prevent an excessive pressure drop across its length.

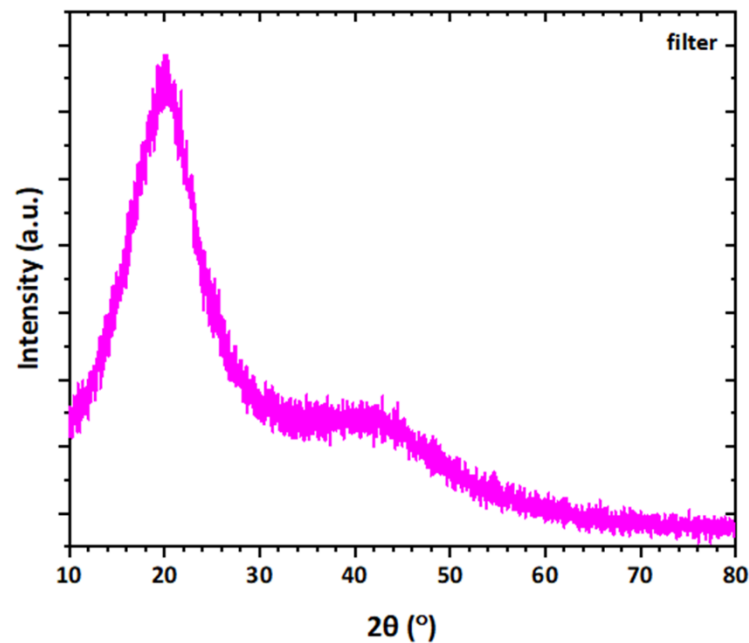


Figure 8. XRD pattern of the modified lattice.

3.4. Raman Analysis

Subsequent examination of the vibrational properties via Raman spectroscopy revealed that the flat filters contained a Bisphenol-based epoxy resin (marked with an asterisk in Figure 9a), a commonly and widely used material in DLP 3D printing. However, additional modes were observed originating from additional monomers and/or the hardener present in the commercial resin solution [41,42]. Moreover, the SiO₂ gel obtained from the dried SiO₂ precursor solution exhibited the characteristic spectrum of the amorphous phase [43].

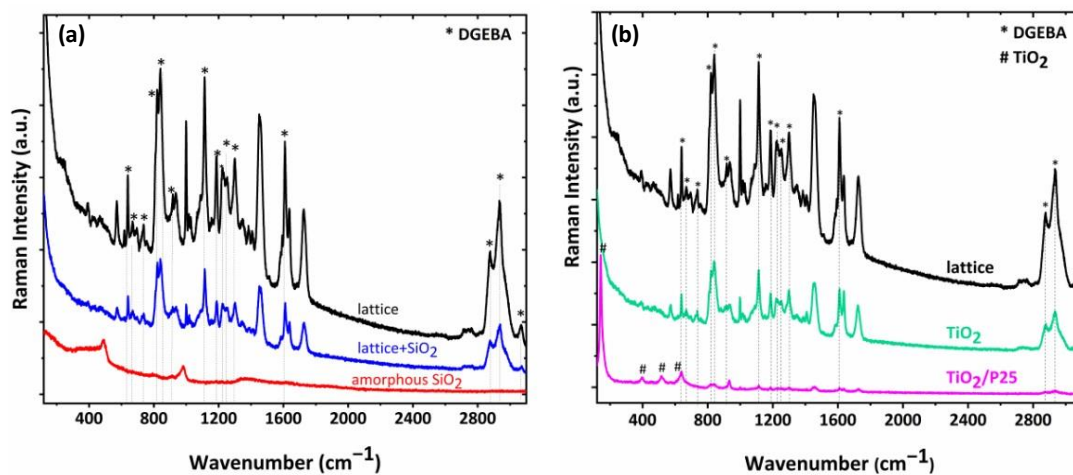


Figure 9. (a) Raman spectra of the developed lattice before and after SiO₂ deposition. In addition, the Raman spectrum of the SiO₂ powder is depicted, obtained after drying the precursor solution utilized for SiO₂ deposition; (b) Raman spectra of the developed lattice before and after the application of TiO₂ and TiO₂/P25 layer coatings onto the lattice.

Consistent with the XRD findings, the deposited silica and titania modes were still undetectable (SiO₂ is in an amorphous phase). However, it should be mentioned that these spectra showed a less intense signal compared to the reference (uncoated) lattice, suggesting that the presence of the additional SiO₂/TiO₂ layers on the lattice surface decreases the intensity of the scattered laser beam. In contrast, the Raman spectra of the

TiO₂/P25 modified lattice exhibited a markedly different pattern, as depicted in Figure 9b; the anatase crystal phase of titania predominated [44], attributable to the high concentration of the commercial P25 photocatalyst, while traces of the most intense epoxy resin modes remained detectable.

3.5. Photocatalytic Performance

As detailed in Section 2.4, photocatalytic degradation tests were conducted against the Triton X-100 surfactant, a common chemical found in polluted wastewater from the steel industry. These tests were performed under UV light irradiation, and the degradation of the pollutant was determined by measuring its characteristic absorption peak at 224 nm. Initially, the UV photolysis of Triton X-100 was conducted using UV-A irradiation without a photocatalyst. After 1.5 h of UV exposure, the degradation of the surfactant was negligible. Subsequently, preliminary experiments employing different nanoparticulate TiO₂ powders under UV-A irradiation for 30 min revealed that the photodegradation of Triton X-100 is more effective with the commercial P25 catalyst, resulting in approximately 60% pollutant removal (Figure 10a). Consequently, it was integrated into an additional final coating on the lattice substrate. At this point, it could be pointed out that Triton X-100 exhibited negligible adsorption onto the surface of the photocatalysts, indicating that the removal effects were solely due to the photocatalytic process.

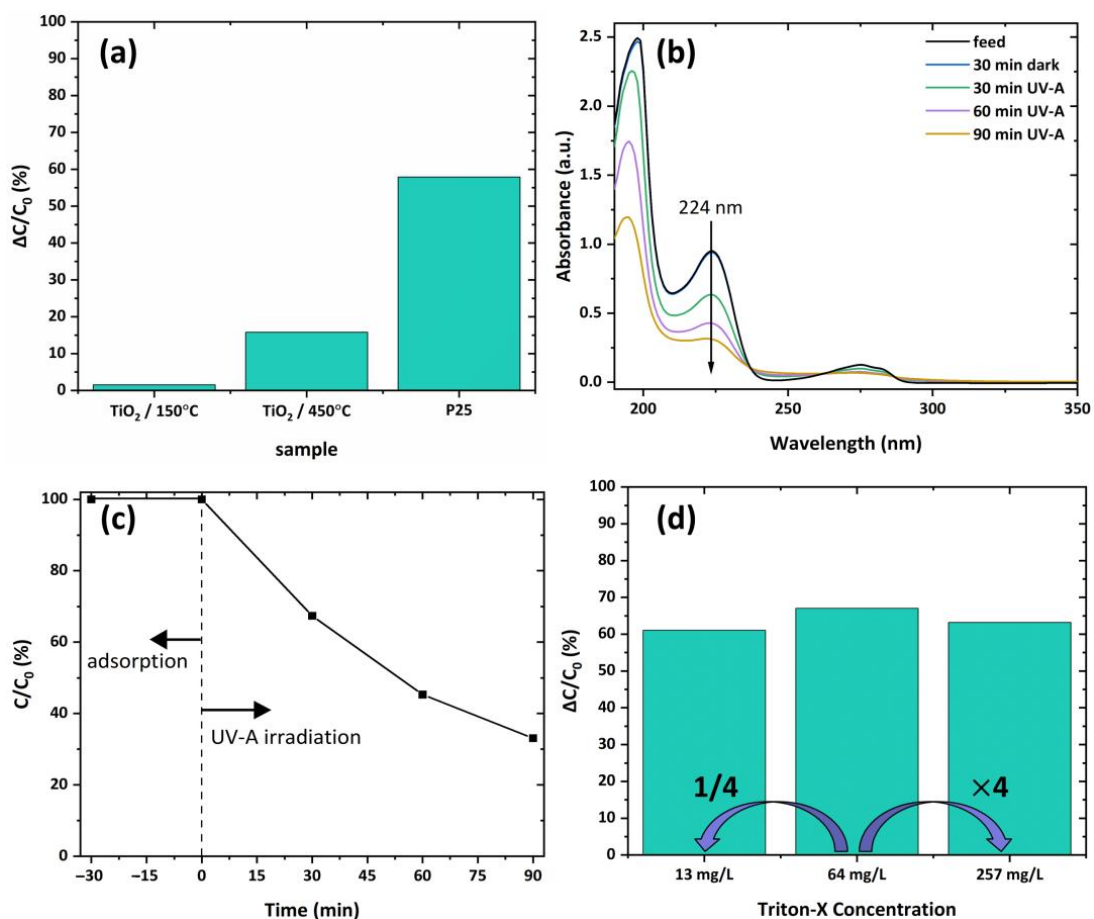


Figure 10. (a) Removal of Triton X-100 at a concentration of 13 mg/L using nanoparticulate TiO₂ powders (catalyst amount: 1 g/L) with UV-A exposure for 30 min (natural pH); (b) evolution of the Triton X-100 UV absorbance at a concentration of 64 mg/L in the supernatant aliquot; (c) study of the kinetics of Triton X-100 (64 mg/L) photocatalytic degradation with TiO₂/P25 thin film on the lattice substrate (natural pH); (d) photocatalytic performance of trilayer-coated lattice as a function of Triton X-100 concentration under UV-A exposure for 90 min (natural pH).

Subsequently, photocatalytic experiments were conducted employing trilayer-coated lattice substrates at a concentration of 64 mg/L under UV-A irradiation for 90 min. As presented in Figure 10b, Triton X-100 can be effectively removed from the solution, as indicated by the decrease in absorbance peak at 224 nm. The results obtained (Figure 10c) demonstrate that the presence of TiO₂/P25 deposited onto the lattice leads to the efficient photocatalytic removal of Triton X-100 pollutant, achieving up to 70% removal.

Simultaneously, the evolution of pH during the photocatalytic experiment was monitored, observing a decrease from 6.5 to 3.3 over time. This pH reduction during the photocatalytic degradation of Triton X-100 by the photocatalyst can be attributed to the generation of acidic species throughout the process. When the photocatalyst is irradiated with UV light, it generates electron–hole pairs (e^-/h^+), which react with water and oxygen in the aqueous solution to produce reactive oxygen species such as hydroxyl radicals ($\cdot\text{OH}$), superoxide anions ($\cdot\text{O}_2^-$), and hydrogen peroxide (H_2O_2) [17]. Triton X-100, a non-ionic surfactant, undergoes oxidation by these reactive oxygen species, resulting in the formation of intermediate products, including various organic acids (e.g., acetic acid, formic acid). These organic acids dissociate in water, releasing hydrogen ions (H^+), which contribute to the observed pH decrease ($\text{R-COOH} \rightarrow \text{R-COO}^- + \text{H}^+$). As the photocatalytic degradation proceeds, additional organic acids are generated and undergo dissociation, leading to an accumulation of H^+ ions in the solution. The continuous production and release of H^+ ions from these acids contribute to a gradual decline in the pH of the solution over time. Additionally, the mineralization of Triton X-100 involves the progressive oxidation of the organic pollutant into CO_2 . The dissolution of CO_2 in water results in the formation of carbonic acid (H_2CO_3), which subsequently dissociates into bicarbonate (HCO_3^-) and hydrogen ions (H^+) ($\text{CO}_2 + \text{H}_2\text{O} \rightarrow \text{H}_2\text{CO}_3 \rightarrow \text{HCO}_3^- + \text{H}^+$). This reaction introduces additional H^+ ions into the solution, thereby further decreasing the pH. The combined effect of the formation of acidic intermediates and the CO_2 dissolution leads to a significant decrease in pH during the photocatalytic process.

Moreover, as exhibited in Figure 10d, the TiO₂/P25 film coating on the lattice substrate efficiently decomposed Triton X-100, irrespective of the initial concentration of the contaminant. It is worth mentioning that the concentration range investigated corresponds to actual levels of Triton X-100 found in the effluents from the steel industry. These results suggest that the immobilized quantity of TiO₂/P25 on the membrane lattices should ideally be at a ratio of 1 g of catalyst per 1 L of wastewater effluent.

Furthermore, the total organic content (TOC) content during photocatalytic experiments was investigated and the results are presented in Figure 11a. As observed, the mineralization of Triton X-100 surfactant exhibits an almost linear relationship with time. Specifically, after 90 min of UV-A irradiation, the carbon content percentage decreases to 58%, indicating that 42% of Triton X-100 has been mineralized. However, the degradation of Triton X-100 was considerably lower, likely due to the formation of intermediate organic products during the process. These intermediates could be more resistant to further breakdown, thereby slowing down the overall mineralization process. While the initial breakdown may occur relatively quickly, the complete oxidation of intermediates to achieve mineralization is slower. Thus, the observed delay in the mineralization process relative to the degree of photocatalytic degradation is expected. The recalcitrant parent compound must first be converted into intermediate fragments, which then progressively transform into CO_2 and inorganic species. This eventually leads to the almost complete removal of the organic load (85%) after 5 h (Figure 11a).

Regarding the recycling study, the photocatalytic activity of the modified lattices was evaluated after they were regenerated by recovering, rinsing with ultrapure water, and drying. Five photocatalysis/regeneration cycles were conducted, and the results are illustrated in Figure 11b. It is apparent that the photocatalytic-modified lattices maintained their high activity, exhibiting only a slight performance decrease of approximately 5.6%.

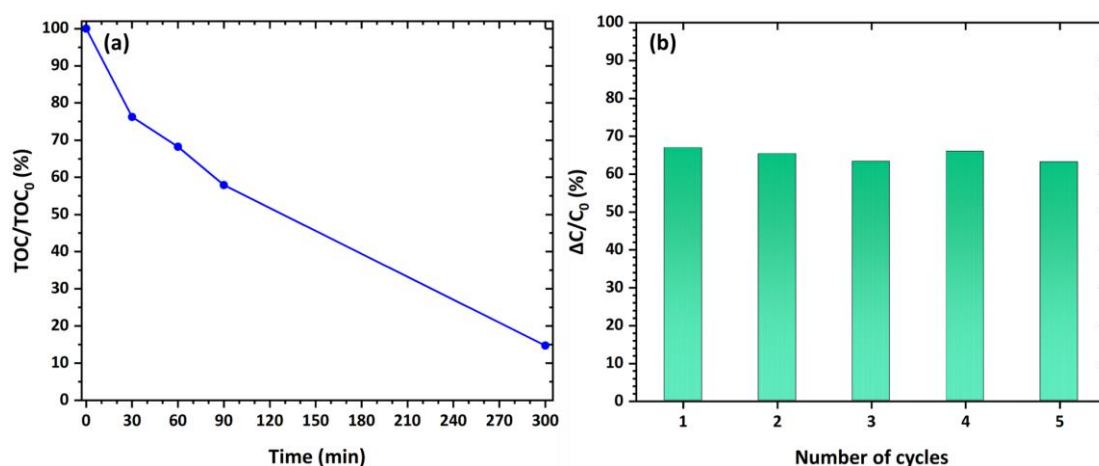


Figure 11. (a) Removal of total organic carbon (TOC) content during the photocatalytic process (UV-A irradiation, catalyst amount = 1 g/L, 64 mg/L pollutant's concentration, natural pH, 25 °C); (b) final rejection of Triton X-100 (%) due to photocatalytic degradation by the modified lattices under UV-A illumination for 90 min, after five successive cycles (initial concentration = 64 mg/L, natural pH, 25 °C).

Overall, the outcomes showcase the advantages and innovation of the proposed 3D-printed photocatalytic reactor technology for water purification. Further experiments are underway to optimize photocatalytic reaction conditions, including the presence of other organic contaminants [45].

4. Conclusions

In this study, flat filters in the form of lattices were fabricated using the 3D printing technique, demonstrating impressive surface area and volume characteristics, suitable for integration into innovative photocatalytic reactors. Through wet chemistry methods, highly uniform, homogeneous, and smooth SiO₂ and TiO₂ layers were prepared without any imperfections. Initially, a silica layer was deposited to insulate and protect the polymer lattice, followed by the application of an outer layer of the titania photocatalyst. Finally, the SiO₂/TiO₂ trilayer displayed exceptional homogeneity and smoothness, covering the entire surface seamlessly.

Both the filters and the trilayer-coated photocatalytic lattices were extensively characterized employing SEM, XRD, and Raman spectroscopy. The TiO₂ photocatalytic activated lattices effectively degraded the Triton X-100 surfactant, a common water pollutant in the steel metal industry, reaching up to 70% removal, regardless of the initial concentration of the contaminant. The concentration range examined aligns with the actual levels of Triton X-100 found in effluents from the steel industry. Moreover, 85% of the organic load was eliminated after 5 h of UV-A irradiation. Overall, the photocatalytic-modified lattices sustained their high activity, exhibiting only a minor performance decrease of approximately 5.6% after five subsequent photocatalysis/regeneration cycles. These findings underscore the advantages of the proposed 3D-printed photocatalytic filtration reactor technology for water purification applications.

Author Contributions: Conceptualization, D.I. and G.E.R.; methodology, G.V.T. and M.K.A.; validation, G.V.T. and M.K.A.; formal analysis, G.V.T. and M.K.A.; investigation, G.V.T. and M.K.A.; resources, G.E.R. and P.F.; writing—original draft preparation, G.V.T.; writing—review and editing, G.E.R.; visualization, G.V.T. and M.K.A.; supervision, P.F.; project administration, T.S.P.; funding acquisition, S.M. and D.I. All authors have read and agreed to the published version of the manuscript.

Funding: This work received funding from the European Union's Horizon 2020 research and innovation programme under grant agreement No 958274 within the framework of iWAYS—Innovative Water recovery Solutions project.

Data Availability Statement: The raw data supporting the conclusions of this article will be made available by the authors on request.

Conflicts of Interest: Author Dimitrios Iatrou was employed by the company IAMAS Technologies Ltd. The remaining authors declare that the research was conducted in the absence of any commercial or financial re-relationships that could be construed as a potential conflict of interest.

References

1. Lin, L.; Yang, H.; Xu, X. Effects of Water pollution on human health and disease heterogeneity: A review. *Front. Environ. Sci.* **2022**, *10*, 880246. [[CrossRef](#)]
2. Chidiac, S.; El Najjar, P.; Ouaini, N.; El Rayess, Y.; El Azzi, D. A comprehensive review of water quality indices (WQIs): History, models, attempts and perspectives. *Rev. Environ. Sci. Biotechnol.* **2023**, *22*, 349–395. [[CrossRef](#)] [[PubMed](#)]
3. Soares, A. Wastewater treatment in 2050: Challenges ahead and future vision in a European context. *Environ. Sci. Ecotechnology* **2020**, *2*, 100030. [[CrossRef](#)] [[PubMed](#)]
4. Kesari, K.K.; Soni, R.; Jamal, Q.M.S.; Tripathi, P.; Lal, J.A.; Jha, N.K.; Siddiqui, M.H.; Kumar, P.; Tripathi, V.; Ruokolainen, J. Wastewater treatment and reuse: A review of its applications and health implication. *Water Air Soil. Pollut.* **2021**, *232*, 208. [[CrossRef](#)]
5. Subramaniam, M.N.; Goh, P.S.; Kanakaraju, D.; Lim, J.W.; Jye, W.J.; Ismail, A.F. Photocatalytic membranes: A new perspective for persistent organic pollutants removal. *Environ. Sci. Pollut. Res.* **2022**, *29*, 12506–12530. [[CrossRef](#)] [[PubMed](#)]
6. Sangamner, R.; Misra, T.; Bherwani, H.; Kapley, A.; Kumar, R. A critical review of conventional and emerging wastewater treatment technologies. *Sustain. Water Resour. Manag.* **2023**, *9*, 58. [[CrossRef](#)]
7. Wang, Y.; Wang, C.; Wang, X.; Qin, H.; Lin, H.; Chhuon, K.; Chen, Q. Research progress of tap water treatment process. *IOP Conf. Ser. Earth Environ. Sci.* **2020**, *546*, 052025. [[CrossRef](#)]
8. Gao, Q.; Li, J.; Jin, P.; Zheng, J.; Xu, D.; Van der Bruggen, B. The practical application value of a sustainable water purification process is crucial. *ACS EST Water* **2023**, *3*, 1990–1993. [[CrossRef](#)]
9. Tian, Y.; Hu, H.; Zhang, J. Solution to water resource scarcity: Water reclamation and reuse. *Environ. Sci. Pollut. Res.* **2017**, *24*, 5095–5097. [[CrossRef](#)] [[PubMed](#)]
10. Fito, J.; Van Hulle, S.W.H. Wastewater reclamation and reuse potentials in agriculture: Towards environmental sustainability. *Environ. Dev. Sustain.* **2021**, *23*, 2949–2972. [[CrossRef](#)]
11. Liao, Z.; Chen, Z.; Xu, A.; Gao, Q.; Song, K.; Liu, J.; Hu, H.-Y. Wastewater treatment and reuse situations and influential factors in major Asian countries. *J. Environ. Manag.* **2021**, *282*, 111976. [[CrossRef](#)] [[PubMed](#)]
12. Silva, J.A. Water supply and wastewater treatment and reuse in future cities: A systematic literature review. *Water* **2023**, *15*, 3064. [[CrossRef](#)]
13. Athanasekou, C.P.; Likodimos, V.; Falaras, P. Recent developments of TiO₂ photocatalysis involving advanced oxidation and reduction reactions in water. *J. Environ. Chem. Eng.* **2018**, *6*, 7386–7394. [[CrossRef](#)]
14. Nasirian, M.; Lin, Y.P.; Bustillo-Lecompte, C.F.; Mehrvar, M. Enhancement of photocatalytic activity of titanium dioxide using non-metal doping methods under visible light: A review. *Int. J. Environ. Sci. Technol.* **2018**, *15*, 2009–2032. [[CrossRef](#)]
15. Chakhtouna, H.; Benzeid, H.; Zari, N.; Qaiss, A.e.k.; Bouhfid, R. Recent progress on Ag/TiO₂ photocatalysts: Photocatalytic and bactericidal behaviors. *Environ. Sci. Pollut. Res.* **2021**, *28*, 44638–44666. [[CrossRef](#)] [[PubMed](#)]
16. Armaković, S.J.; Savanović, M.M.; Armaković, S. Titanium dioxide as the most used photocatalyst for water Purification: An overview. *Catalysts* **2023**, *13*, 26. [[CrossRef](#)]
17. Theodorakopoulos, G.; Athanasekou, C.; Romanos, G.E.; Papageorgiou, S.K. Current photocatalytic systems for intensified water purification applications. In *Handbook of Smart Photocatalytic Materials*, 1st ed.; Hussain, C.M., Mishra, A.K., Eds.; Elsevier: Amsterdam, The Netherlands, 2020; pp. 231–264.
18. Pelaez, M.; Nolan, N.T.; Pillai, S.C.; Seery, M.K.; Falaras, P.; Kontos, A.G.; Dunlop, P.S.M.; Hamilton, J.W.J.; Byrne, J.A.; O’Shea, K.; et al. A review on the visible light active titanium dioxide photocatalysts for environmental applications. *Appl. Catal. B-Environ.* **2012**, *125*, 331–349. [[CrossRef](#)]
19. Moustakas, N.G.; Katsaros, F.K.; Kontos, A.G.; Romanos, G.E.; Dionysiou, D.D.; Falaras, P. Visible light active TiO₂ photocatalytic filtration membranes with improved permeability and low energy consumption. *Catal. Today* **2014**, *224*, 56–69. [[CrossRef](#)]
20. Athanasiou, D.A.; Romanos, G.E.; Falaras, P. Design and optimization of a photocatalytic reactor for water purification combining optical fiber and membrane technologies. *Chem. Eng. J.* **2016**, *305*, 92–103. [[CrossRef](#)]
21. Nakano, K.; Obuchi, E.; Takagi, S.; Yamamoto, R.; Tanizaki, T.; Taketomi, M.; Eguchi, M.; Ichida, K.; Suzuki, M.; Hashimoto, A. Photocatalytic treatment of water containing dinitrophenol and city water over TiO₂/SiO₂. *Sep. Purif. Technol.* **2004**, *34*, 67–72. [[CrossRef](#)]
22. Mozia, S.; Brożek, P.; Przepiórski, J.; Tryba, B.; Morawski, A.W. Immobilized TiO₂ for phenol degradation in a pilot-scale photocatalytic reactor. *J. Nanomater.* **2012**, *2012*, 949764. [[CrossRef](#)]
23. Rezaei, M.; Rashidi, F.; Royae, S.J.; Jafarikoju, M. Performance evaluation of a continuous flow photocatalytic reactor for wastewater treatment. *Environ. Sci. Pollut. Res.* **2014**, *21*, 12505–12517. [[CrossRef](#)] [[PubMed](#)]

24. Jawad, A.H.; Mubarak, N.S.A.; Ishak, M.A.M.; Ismail, K.; Nawawi, W.I. Kinetics of photocatalytic decolourization of cationic dye using porous TiO₂ film. *J. Taibah Univ. Sci.* **2016**, *10*, 352–362. [[CrossRef](#)]
25. Abdel-Maksoud, Y.; Imam, E.; Ramadan, A. TiO₂ solar photocatalytic reactor systems: Selection of reactor design for scale-up and commercialization—Analytical review. *Catalysts* **2016**, *6*, 138. [[CrossRef](#)]
26. Phan, D.D.; Babick, F.; Trinh, T.H.T.; Nguyen, M.T.; Samhaber, W.; Stintz, M. Investigation of fixed-bed photocatalytic membrane reactors based on submerged ceramic membranes. *Chem. Eng. Sci.* **2018**, *191*, 332–342. [[CrossRef](#)]
27. Al-Mamun, M.R.; Kader, S.; Islam, M.S. Solar-TiO₂ immobilized photocatalytic reactors performance assessment in the degradation of methyl orange dye in aqueous solution. *Environ. Nanotechnol. Monit. Manag.* **2021**, *16*, 100514.
28. Wang, D.; Mueses, M.A.; Márquez, J.A.C.; Machuca-Martínez, F.; Grčić, I.; Moreira, R.P.M.; Li Puma, G. Engineering and modeling perspectives on photocatalytic reactors for water treatment. *Water Res.* **2021**, *202*, 117421. [[PubMed](#)]
29. Le, C.; Wismer, M.K.; Shi, Z.-C.; Zhang, R.; Conway, D.V.; Li, G.; Vachal, P.; Davies, I.W.; MacMillan, D.W.C. A general small-scale reactor to enable standardization and acceleration of photocatalytic reactions. *ACS Cent. Sci.* **2017**, *3*, 647–653. [[CrossRef](#)] [[PubMed](#)]
30. Janczarek, M.; Kowalska, E. Computer simulations of photocatalytic reactors. *Catalysts* **2021**, *11*, 198. [[CrossRef](#)]
31. Ballari, M.d.l.M.; Alfano, O.M.; Cassano, A.E. Mass transfer limitations in slurry photocatalytic reactors: Experimental validation. *Chem. Eng. Sci.* **2010**, *65*, 4931–4942. [[CrossRef](#)]
32. Yao, Y.; Zheng, Y.; Yang, Y. Numerical simulation of energy and mass transfer in a magnetic stirring photocatalytic reactor. *Sustainability* **2023**, *15*, 7604. [[CrossRef](#)]
33. Xiao, M.; Wang, Z.; Maeda, K.; Liu, G.; Wang, L. Addressing the stability challenge of photo(electro) catalysts towards solar water splitting. *Chem. Sci.* **2023**, *14*, 3415. [[CrossRef](#)] [[PubMed](#)]
34. Alalm, M.G.; Djellabi, R.; Meroni, D.; Pirola, C.; Bianchi, C.L.; Boffito, D.C. Toward scaling-up photocatalytic process for multiphase environmental applications. *Catalysts* **2021**, *11*, 562. [[CrossRef](#)]
35. Isopencu, G.O.; Mocanu, A.; Deleanu, I.-M. A brief review of photocatalytic reactors used for persistent pesticides degradation. *ChemEngineering* **2022**, *6*, 89. [[CrossRef](#)]
36. Yang, H.; Lee, Y.-J.; Park, S.-J.; Lee, C.-G. Exploring the viability of a floating photocatalyst in a continuous stirred tank reactor system for continuous water treatment. *Environ. Sci. Pollut. Res.* **2023**, *30*, 114582–114590. [[CrossRef](#)] [[PubMed](#)]
37. Ye, L.; Zhang, Y.; Zhang, X.; Hu, T.; Ji, R.; Ding, B.; Jiang, B. Sol-gel preparation of SiO₂/TiO₂/SiO₂-TiO₂ broadband antireflective coating for solar cell cover glass. *Sol. Energy Mater. Sol. Cells* **2013**, *111*, 160–164. [[CrossRef](#)]
38. Du, P.; Carneiro, J.T.; Moulijn, J.A.; Mul, G. A novel photocatalytic monolith reactor for multiphase heterogeneous photocatalysis. *Appl. Catal. A: Gen.* **2008**, *334*, 119–128. [[CrossRef](#)]
39. Vodišek, N.; Ramanujachary, K.; Brezová, V.; Štangar, U.L. Transparent titania-zirconia-silica thin films for self-cleaning and photocatalytic applications. *Catal. Today* **2017**, *287*, 142–147.
40. Theodorakopoulos, G.V.; Arfanis, M.K.; Sánchez Pérez, J.A.; Agüera, A.; Cadena Aponte, F.X.; Markellou, E.; Romanos, G.E.; Falaras, P. Novel pilot-scale photocatalytic nanofiltration reactor for agricultural wastewater treatment. *Membranes* **2023**, *13*, 202. [[CrossRef](#)] [[PubMed](#)]
41. de Andrade, J.E.; Machado, R.; Macêdo, M.A.; Cunha, C.; Guilherme, F. AFM and XRD characterization of silver nanoparticles films deposited on the Surface of DGEBA epoxy resin by ion sputtering. *Polímeros* **2013**, *23*, 19–23. [[CrossRef](#)]
42. Farquharson, S.; Smith, W.W.; Rose, J.; Shaw, M. Correlations between molecular (raman) and macroscopic (rheology) data for process monitoring of thermoset composites. *JPACSM Process Anal. Chem.* **2002**, *7*, 45–53.
43. Degioanni, S.; Jurdyc, A.M.; Cheap, A.; Champagnon, B.; Bessueille, F.; Coulm, J.; Bois, L.; Vouagne, D. Surface-enhanced Raman scattering of amorphous silica gel adsorbed on gold substrates for optical fiber sensors. *J. Appl. Phys.* **2015**, *118*, 153103. [[CrossRef](#)]
44. Arfanis, M.K.; Adamou, P.; Moustakas, N.G.; Triantis, T.M.; Kontos, A.G.; Falaras, P. Photocatalytic degradation of salicylic acid and caffeine emerging contaminants using titania nanotubes. *Chem. Eng. J.* **2017**, *310*, 525–536. [[CrossRef](#)]
45. Saien, J.; Ojaghloo, Z.; Soleymani, A.R.; Rasoulifard, M.H. Homogeneous and heterogeneous AOPs for rapid degradation of Triton X-100 in aqueous media via UV light, nano titania hydrogen peroxide and potassium persulfate. *Chem. Eng. J.* **2011**, *167*, 172–182. [[CrossRef](#)] [[PubMed](#)]

Disclaimer/Publisher’s Note: The statements, opinions and data contained in all publications are solely those of the individual author(s) and contributor(s) and not of MDPI and/or the editor(s). MDPI and/or the editor(s) disclaim responsibility for any injury to people or property resulting from any ideas, methods, instructions or products referred to in the content.